LC-DET-2001-042

A Pixel Vertex Tracker for the TESLA Detector

M. Battaglia

CERN, Geneva (Switzerland) and
Dept. of Physics, University of Helsinki (Finland)

S. Borghi and R. Campagnolo

Dip. di Fisica, Universita' degli Studi and INFN, Milano (Italy)

M. Caccia

Dip. di Scienze, Universita' dell'Insubria and INFN, Como (Italy)

K. Domanski, P. Grabiec, B. Jaroszewicz,
J. Marczewski, D. Tomaszewski

Institute of Electron Technology, Warszawa (Poland)

W. Kucewicz

Dept. of Electronics, University of Mining and Metallurgy, Krakow (Poland)

A. Zalewska

High Energy Physics Lab., Institute of Nuclear Physics, Krakow (Poland)

K. Tammi

Helsinki Institute of Physics (Finland)

Abstract

In order to fully exploit the physics potential of a e^+e^- linear collider, such as TESLA, a Vertex Tracker providing high resolution track reconstruction is required. Hybrid Silicon pixel sensors are an attractive sensor technology option due to their read-out speed and radiation hardness, favoured in the high rate TESLA environment, but have been so far limited by the achievable single point space resolution. A novel layout of pixel detectors with interleaved cells to improve their spatial resolution is introduced and the results of the characterisation of a first set of test structures are discussed. In this note, a conceptual design of the TESLA Vertex Tracker, based on hybrid pixel sensors is presented.

1 Introduction

The next generation of high energy e^+e^- experiments, following the LEP and SLC programs, will be at a linear collider. The TESLA concept, based on super-conducting accelerating structures, will be able to deliver luminosities in excess to 10^{34} cm^{-2} s^{-1}, at centre-of-mass energies ranging from the Z^0 pole up to about 1 TeV. Such a collider will naturally complement the physics reach of the Tevatron and LHC hadron colliders in the study of the mechanism of electro-weak symmetry breaking and in the search for new physics beyond the Standard Model. Both precision measurements and particle searches set stringent requirements on the efficiency and purity of the flavour identification of hadronic jets since final states including short-lived b and c-quarks and τ leptons are expected to be the main signatures. High accuracy in the reconstruction of the charged particle trajectories close to their production point is required in order to reconstruct the topologies of the secondary vertices in the decay chain of short-lived heavy flavour particles.

If a light, elementary Higgs boson exists, as indicated by the LEP, SLD and LEP-2 data, it will be essential to carry out precision measurements of its couplings to the different fermion species as a proof of the mass generation mechanism and in order to identify its Standard Model or Supersymmetric nature [1]. This can be achieved by accurate determinations of its decay rate to $b\bar{b}$, $c\bar{c}$, $\tau^+\tau^-$, W^+W^- and gluon pairs to detect possible deviations from the Standard Model predictions. Since the rates for the Higgs boson decay modes into lighter fermions $H^0 \to c\bar{c}$, $\tau^+\tau^-$ or into gluon pairs are expected to be only about 10% or less of that for the dominant $H^0 \to b\bar{b}$ process, the extraction and measurement of these signals require the suppression of the $b\bar{b}$ contribution by a factor of twenty or better, while preserving a good efficiency.

The measurement of the Higgs-top Yukawa coupling as well as that of the top-quark mass will also require efficient b-tagging to reduce the combinatorial background in the reconstruction of the six and eight jet final states. If Supersymmetry is realized in nature, the study of its rich Higgs sector will also depend upon the efficient identification of b jets and τ leptons to isolate the signals for the decays of the heavier A^0, H^0 and $H^\pm$ bosons from the severe combinatorial backgrounds in the complex multi-jet hadronic final states. Due to the expected large b jet multiplicity, highly efficient tagging is required to preserve a sizeable statistics of the signal events. Finally, both b and c-tagging will be important in the study of the quark scalar partners, while τ identification may be instrumental in isolating SUSY signals in large $\tan\beta$ scenarios and Gauge Mediated Supersymmetry Breaking models.

In order to correlate the track extrapolation accuracy to the performances of a jet flavour tagging algorithm at the linear collider, Figure 1 shows the c / b quark separation capabilities under different assumptions for the track impact parameter resolution.

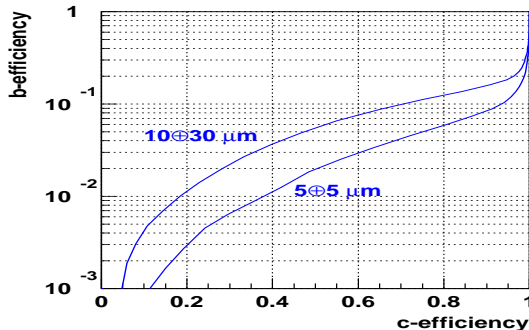While the developments of Vertex Trackers from the LEP and SLD experiments to

Figure 1: *The b-quark background efficiency as a function of the c-quark signal efficiency for a c-tag algorithm based on topological vertexing and impact parameters, developed on the basis of the experience from the SLC and LEP experiments (from [2]). The two curves show the expected performance for two different assumptions on the track impact parameter resolution.*

those at B-factories, the Tevatron and the LHC have addressed many crucial aspects, such as radiation hardness, read-out speed and the considerable size increase of the trackers, the impact parameter (*i.p.*) resolution, σ_{ip}, has not benefited of significant improvements. Limited in terms of multiple scattering at B factories and by radiation damage in their closest approach to the beam at hadron colliders, the typical performances are comparable to those achieved at LEP: $\sigma_{ip} = 25 \ \mu\text{m} \oplus 70 \ \mu\text{m}/p_t \ \text{GeV}/c$. In order to fulfil its challenging requirements, the TESLA Vertex Tracker aims at significantly improving on the already outstanding SLD VXD3 performances of $8 \ \mu\text{m} \oplus 33 \ \mu\text{m}/p_t$ GeV/c [3]. An improvement to σ_{ip} to $5 \ \mu\text{m} \oplus 10 \ \mu\text{m}/p_t$ GeV/c corresponds to a factor $\simeq 2$ increase in charm jet tagging efficiency and a factor $\simeq 1.25$ increase in beauty jet tagging efficiency at constant mis-identification probability. A precise determination of the track perigee parameters close to their production point also assists in the track reconstruction and improves the momentum resolution for charged particles.

The design of the TESLA Vertex Tracker and the choice of the sensor technology are driven by these requirements, to be achieved within the constraints set by the accelerator induced backgrounds at the interaction region and by the characteristics of the physics events. In the next section, the conceptual design proposed for the Vertex Tracker of the TESLA detector is presented while Section 3 reviews its expected performances. In Section 4, the silicon pixel sensor design, developed to overcome the hybrid pixel sensor limitations in terms of single point space resolution is discussed in details. A road-map of dedicated R&D activity, to validate the concepts presented, concludes.

2   Vertex Tracker Conceptual Design

The proposed Vertex Tracker geometry consists of three layers of pixel detectors, providing at least three space points for charged particles with polar angles down to $|\cos\theta|$ = 0.995. In order to optimise the amount of material traversed by the particles and their angle of incidence on the sensitive plane, the outermost layer is split into a barrel section and a forward crown as shown in Figure 2. A GEANT model of this geometry has been implemented in the BRAHMS simulation program [11] and used for its optimisation and the evaluation of the performances in terms of the impact parameter resolution as discussed in Section 4. The radial position of the innermost layer is set at 1.5 cm by the beam-pipe radius, limited to 1.4 cm due to constraints on the design of the machine collimation system. The outermost layer has been positioned at a radius of 10 cm, fitting the proposed general detector concept that includes two further silicon detector layers located between the Vertex Tracker and the TPC main tracker. The number of additional intermediate layers is limited by the multiple scattering.
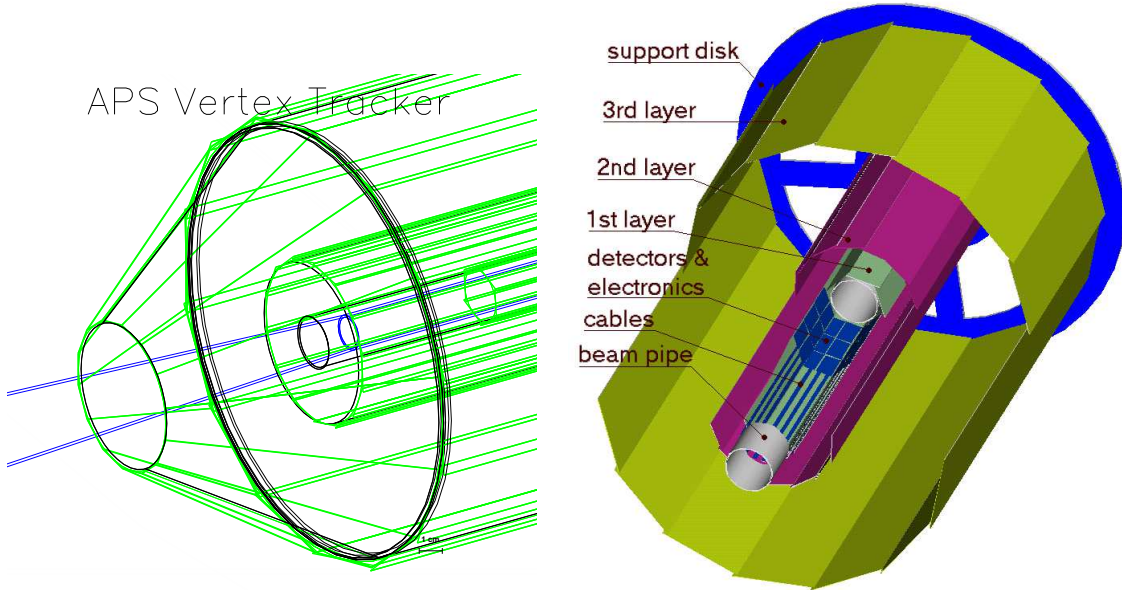

Figure 2: *A view of the proposed silicon Vertex Tracker with three concentric layers as implemented in the* GEANT *(left) and* CAD *(right) models. A forward crown of detector is attached at both ends on the carbon fibre support structure.*

Detailed simulation studies, assuming a layer efficiency of 97%, have shown that an optimal configuration consists of one intermediate layer located at 3.5 cm, this layer assisting the extrapolation to the innermost layer affected by the higher occupancy and supplementing a space point close enough to the interaction point in cases of failures

on the first layer. Overlaps of neighbouring detector modules provide an useful mean to verify their relative alignment using particle tracks from dedicated calibration runs, taken at Z centre-of-mass energy.

The limitation in the amount of material traversed by charged particles being a major concern to minimise the multiple scattering effects, the pixel Vertex Tracker requires a light support structure able to cope with the load of the detector plaquettes and to ensure their stability to better than their intrinsic single point resolution. The proposed concept for the mechanical structure envisages the use of diamond-coated thin carbon fibre support shells, acting also as heat pipes to extract the heat dissipated by the read-out electronics, uniformly distributed over the whole active surface of the detector. A support plate at each end of the barrel section, made of two thin carbon fibre skins glued together by means of small spacers ensures the needed rigidity and provides a routing for the cables and a support for the forward crown (see Figure 3).
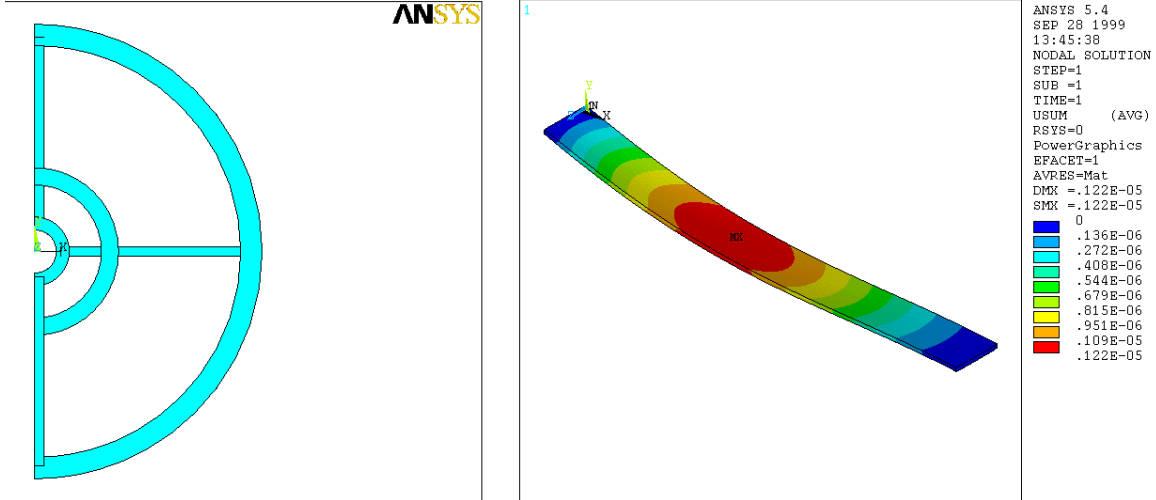

Figure 3: *Left: The carbon fibre end-plate support structure and Right: result of a finite element analysis of the deformations induced on a detector module due to the temperature gradient. The module is fixed at both ends and the largest displacement corresponds to 10 μm for the innermost layer.*

Assuming a power dissipation of 40 μW/channel, the total heat flux is 790 W, corresponding to 2600 W/m^2, for a read-out pitch of 100 μm. In presence of a power dissipation Q, the temperature gradient along the silicon sensor ΔT scales as $\Delta T = \frac{Q\ell^2}{2kt}$, where ℓ is the distance, t the sensor thickness and k the thermal conductivity. Owing to its high thermal conductivity (1000-2000 W/m K), small thermal expansion ($\simeq 2 \times 10^{-6}$ $^{\circ}C^{-1}$), high electrical resistivity and large radiation length X_0, diamond is particularly well suited as a heat pipe material. The envisaged cooling scheme consists of a diamond

coated heat pipe integrated onto the support layer and heat drains regularly spaced. These drains, consisting of pipes circulating liquid coolant, must be placed every 5 cm along the longitudinal coordinate, except for the innermost layer where they can be placed only at the detector ends to minimise the amount of material. The low duty cycle of the accelerator, makes interesting to consider pulsed power operation to reduce power dissipation.

Signals can be routed along the beam pipe and the end-cap disks to the repeater electronics installed between the vertex detector and the forward masks which shield the detector from background. The material budget has been estimated by assuming 200 μm thick detectors and back-thinning of the read-out chip to 50 μm, corresponding to 0.3 % X_0, and the support structure. It corresponds to 1.6 % X_0 for the full tracker (see Figure 4 and Table 1).
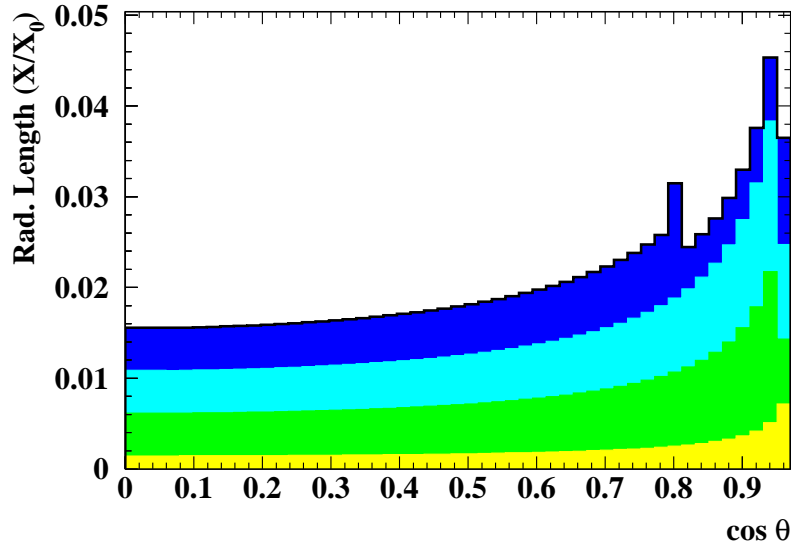

Figure 4: *The material budget, in units of radiation length, for the proposed pixel Vertex Tracker as a function of the polar angle. The contribution from the Be beam-pipe and those of the three layers are shown from bottom to top respectively. The adoption of a forward crown of detectors to complement the barrel section of the tracker allows to minimize the rise of the material traversed by particles produced at the interaction region at low angles.*

The expected data size from the Vertex Tracker has been computed assuming 600 hits per bunch crossing from background sources and 50 charged particles. Taking 16 bits per pixel, this corresponds to 150 kbyte of data from the Vertex Tracker per

	R (cm)	Material	X (cm)	X_0 (cm^{-1})	X/X_0 (%)
Beam-pipe	1.4	Be	0.0500	35	0.15
Sensor+VLSI+Kapton	1.5	Si	0.0250	9.4	0.37
Support	1.2	CF	0.0240	25	0.10
Sensor+VLSI+Kapton	3.5	Si	0.0250	9.4	0.37
Support	3.5	CF	0.0240	25	0.10
Sensor+VLSI+Kapton	10.0	Si	0.0250	9.4	0.37
Support	10.0	CF	0.0240	25	0.10
Total					1.60

Table 1: *The material budget for the pixel Vertex Tracker with the detailed contributions from its different components.*

e^+e^- event.

3 Simulation Studies and Vertex Tracker Performances

The performances of the pixel Vertex Tracker have been evaluated for $e^+e^- \rightarrow HZ \rightarrow q\bar{q}\ell^+\ell^-$ and $e^+e^- \rightarrow t\bar{t} \rightarrow W^+bW^-\bar{b}$ events at $\sqrt{s} = 350$ and 500 GeV using full GEANT simulation. Tracks reconstructed in the TPC TESLA main tracker have been extrapolated to the detector planes of the pixel Vertex Tracker and a dedicated pattern recognition program has been used to define the association of the recorded hits to the extrapolated tracks. While no attempt has been made to define local track element using only the three layers of the Vertex Tracker, these can be efficiently defined by adding the hits on the two layers of the Silicon Intermediate Tracker, foreseen at radii of 16 and 30 cm. The impact parameter resolution has been studied as a function of the Vertex Tracker geometry, namely the radial position of the second layer, and of the assumed single point resolution σ_{point}. Results are summarised in Tables 2 and 3. The efficiency for associating at least two hits to an extrapolated charged particle with $p > 1$ GeV/c has been found to be $\simeq 95\%$. The track fit has been performed using a Kalman-filter [12] and the impact parameter resolution has been obtained from the estimated covariance matrix. The results obtained assuming $\sigma_{point} = 7$ μm, are shown in Figure 5.

σ_{point} (μm)	$\sigma_{IP}^{asymptotic}$ (μm) $(R - \phi)$
4.	3.7
7.	5.3
10.	7.5
13.	9.5

Table 2: *Observed variation of the asymptotic impact parameter resolution for different values of the assumed detector single point resolution.*

R_2 (cm)	Asymptotic σ_{IP} $(R - \phi)$ (μm)	Fraction of Tracks in Tails
7.5	6.0	12 %
5.5	5.6	7 %
3.5	5.2	4 %

Table 3: *Observed variation of the asymptotic impact parameter resolution and the fraction of tracks in the non-Gaussian tails of the resolution function for different values of the assumed radial position R_2 of the second Vertex Tracker layer.*
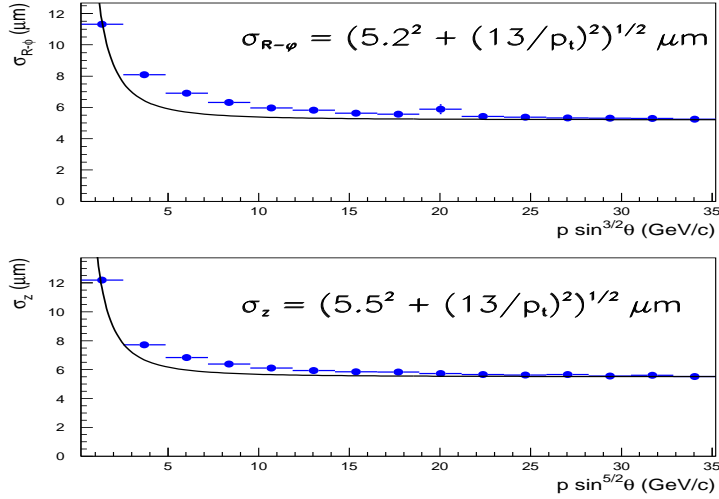

Figure 5: *Impact parameter resolution in the $R - \phi$ (upper plot) and $R - z$ (lower plot) projections for particles as a function of their momentum and polar angle.*

4 Hybrid Pixel Sensors

The main requirements for the Vertex Tracker sensors may be summarised as follows:

- A single point resolution ≤ 7 μm and a thickness of ≤ 200 μm to attain the required impact parameter resolution.

- Time stamping capabilities to identify particles originating from a single bunch crossing, occurring at TESLA every 337 (189) ns at $\sqrt{s} = 500$ (800) GeV to reduce the pair background and the number of $\gamma\gamma \rightarrow$ hadrons events overlapped to the products of a e^+e^- collision.

- A sensitive cell area below $150 \times 150 \mu$m^2 to keep the occupancy from backgrounds and dense hadronic jets below 1%.

At present, two silicon sensor technologies have the potential to satisfy these specifications: monolithic (Charged Coupled Devices (CCD) and CMOS imagers) and hybrid pixels sensors. Hybrid pixel sensors have the advantage of allowing fast time stamping and sparse data scan read-out, thereby reducing the occupancies due to backgrounds, and of being tolerant to neutron fluxes well beyond those expected at the linear collider. Both these characteristics have been demonstrated for their application in the LHC experiments. However, improvements in the pixel sensor spatial resolution and a reduction of the sensor total thickness are needed. These represent areas of R&D that are specific to this linear collider application. CCD require a complementary development. Their readout speed and radiation tolerance need to be improved, their resolution and thickness being already close to requirements. CMOS imagers have recently appeared and could overcome the CCD limitations while offering similar advantages.

A single point precision at the 5 μm level can be obtained by sampling the diffusion of the carriers generated along the particle path and adopting an analog read-out to interpolate the signals of neighbouring cells. Since the charge diffusion r.m.s. is ≈ 8 μm in 300 μm thick silicon, an efficient sampling requires a pixel pitch well below 50 μm. At present, the most advanced pixel read-out electronics have minimum cell dimension of $50 \times 300 \mu$m^2, limiting an efficient signal interpolation. Even if a sizeable reduction in the cell dimension may be envisaged by the deep submicron trend in the VLSI development, a sensor design overcoming such basic limitation is definitely worth being explored.

4.1 Detector design and first prototype production

The pixel detector design discussed here exploits a layout inherited from the microstrip detectors [4] where it is assumed to have a read-out pitch n times larger than the pixel

pitch. The proposed sensor layout is shown in Figure 6 for n=4. In such a configuration, the charge carriers created underneath an interleaved pixel will induce a signal on the output nodes, capacitively coupled to the interleaved pixel. In a simplified model
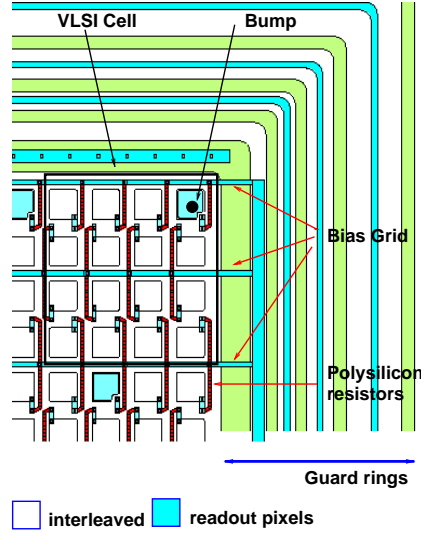

Figure 6: *Layout of the proposed detector, corresponding to a 50 μm pitch in both dimensions; the other structures differ by the pitch only*

where the detector is reduced to a capacitive network, the ratio of the signal amplitudes on the output nodes at the left hand side and right hand side of the interleaved pixel (in both dimensions) should have a linear dependence on the particle position. The ratio between the inter-pixel capacitance and the pixel capacitance to backplane plays a crucial role in the detector design, as it defines the signal amplitude reduction at the output nodes and therefore the maximum sustainable number of interleaved pixels. Recently published results on 200 μm readout pitch microstrip detectors have demonstrated a 10 μm resolution for a layout with three interleaved strips (50 μm strip pitch) and S/N ≈ 80 [5]. Similar results may be expected in a pixel detector, taking into account that a lower noise is achievable due to the intrisically smaller load capacitance and that the charge sharing on four output nodes makes possible to reconstruct the particle position in two dimensions. Further improvements are possible by sampling the charge carrier diffusion at a smaller pitch.

Prototypes of detectors with interleaved pixels have been designed and manufactured. The layout of one of the structures is shown in Figure 6. A series of guard rings defines the detector sensitive area. A bias grid allows the polarization of the interleaved pixels too; each p^+ implant is connected to the metal bias line by polysilicon resistors in the $1 - 3$ MΩ range. A metal layer is deposited on top of the pixels to be connected to the VLSI cell. The backplane has a meshed metal layer to allow the use

of an IR diode for charge collection studies. In a 4", 350 μm thick, wafer 36 structures were fit, for 17 different layouts; a VLSI cell of 200×200 μm^2 or 300×300 μm^2 was assumed and detectors with a number of interleaved pixels ranging between 0 and 3 and different areas were designed.

Ten high resistivity wafers ($5 - 8$ kΩcm) were processed together with an equal number of low resistivity wafers for process control [6]. The technological sequence may be outlined as follows [7]:

- wafer oxidation by HCl gettering, to form a 700 nm thick Silicon dioxide layer;

- Phosphorus glass deposition from a POCl$_3$ source followed by drive-in in oxidizing environment. The P diffusion was meant to form an n$^+$ layer on the backplane, to guarantee a good ohmic contact with the metal grid;

- pixel and guard ring window opening in the photomask, applying a wet etching technique;

- Boron diffusion, followed by a drive-in process. The resulting junctions were 0.7μm deep;

- high quality thin oxide (200 nm) growth at 1000 ºC to define the integrated coupling capacitor on every pixel. This step was carefully monitored to achieve an extremely low density of mobile ion charge;

- polysilicon layer deposition (500 nm thick) and implantation, for the bias resistors. A special high temperature annealing was optimised to obtain the required sheet resistence 250kΩ;

- resistor pattern definition by photolitography;

- planarisation by BPSG (Boron-Phosphorus-Silicon Glass) chemical vapour deposition, followed by a high temperature annealing;

- resistor coating by photolitography, applying plasma and wet etching technique;

- definition of the contact window between the resistors and the p$^+$ implants. To decrease the contact resistence, Boron implantation was used;

- metal deposition by sputtering a 1.2μm thick Al-Si-Cu layer, patterned by photolitography and plasma etching;

- backside metallisation grid by Al evaporation and plasma etching

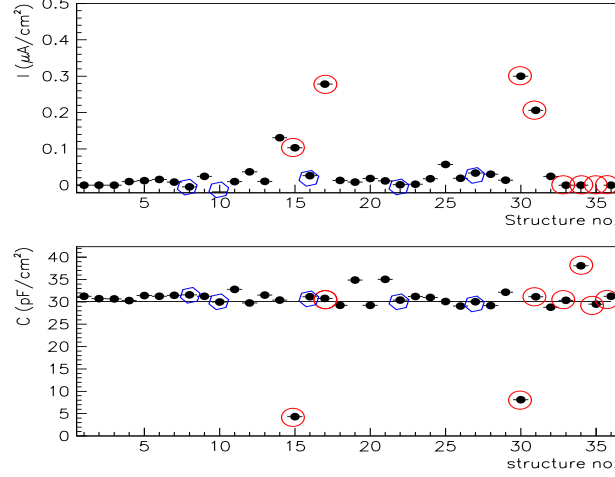- final wafer sintering in Hydrogen at 450 ºC for 20'.

Figure 7: *Leakage current and capacitance at full depletion voltage for all of the 36 structures in one of the good wafers; circles define the detectors rejected because of breakdowns below* 100 V*; hexagons identify rejected detectors because of interrupted metal lines. The line corresponds to the expected capacitance per unit area.*

Standard cleaning was performed before each high temperature step. After the processing, two wafers were retained by the factory for a destructive analysis and two others were stored for later use. All of the structures on the available wafers were visually inspected, tested up to 250 V and characteristics I-V and C-V curves produced. In Figure 7 the value of the currents and detector capacitances at depletion voltage are shown for all of structures in one of the wafers. In Figure 8 the typical I vs. V and $1/C^2$ vs. V curves of a good structure are shown. While the C vs. V curves behave as expected, the current has a peculiar trend. After a plateau is reached at full depletion, the current increases significantly at $V = 50 - 70$ V. For most of the structures this is a mild increase, but most of the rejected detectors are characterized by a steep slope, eventually resulting in a breakdown for values of the reverse bias voltage below 100 V. Independent measurements of the guard ring and bias grid current have shown the latter to be responsible for this effect, possibly due to sharp edges where the electric field achieves high values. The average yield over the tested wafers is about 50%; most of the rejected structures feature either an early breakdown or an extremely high leakage current, independent of the applied voltage, correlated to surface defects possibly associated to the plasma etching of the Al pattern. An improvement in the technology sequence, requiring a better planarisation and avoiding plasma etching has been agreed with the manufacturer. Good structures are characterised by a leakage current at the $10 \mathrm{nA/cm^2}$ level and backplane capacitances in agreement to the expectations.
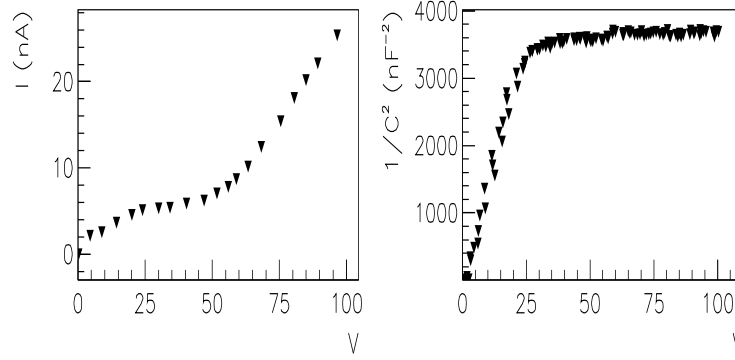
Figure 8: I vs. V and $1/C^2$ vs. V curves for a typical good detector

4.2 Interpixel and backplane capacitance simulation and measurements

In order to study the charge collection properties of the proposed detector, a detailed characterization of its electrostatic properties is necessary. In a simplified model, the detector may be reduced to a capacitive network. Each pixel is a node characterised by the backplane capacitance (C_{bp}) and the inter-pixel capacitances (C_{ip}), dominated by the couplings to the nearest and diagonal neighbours. The C_{ip}/C_{bp} ratio is crucial in the detector design, as it defines the signal amplitude reduction (an effective charge loss) at the output nodes. In order to be able to evaluate the expected behaviour of the prototypes, the capacitances were measured and calculated. Moreover, the obtained values were used as input for a network analysis providing an estimate of the charge loss. Since single pixel capacitances are expected to be at the 10 fF level, the measurement conditions were optimised as follows:

- The capacitance was measured using a Hewlett-Packard 4280 CV meter, operating at 1 MHz. A cable correction procedure accounting for finite admittances to ground was used. Moreover, an open circuit correction was applied, measuring the capacitance with raised probe tips.

- All pixels along a single metal bias line were set in parallel, isolating the line from the bias grid (see Figure 6). The number of pixels along a line ranges between 64 and 254, depending on the pixel pitch, thus increasing the measured capacitance values to 0.5-2 pF.

- For every structure, three bias lines were isolated and the capacitance for each of

13

them, for three doublets in parallel and for one triplet was measured. The offset in the linear regression for the capacitance versus the number of lines measured the left-over parasitic contributions after the cable correction.

- For each structure, independent measurements of the total interpixel capacitance and of the sum of the interpixel and backplane capacitance were done.

The numerical estimate is essential to break down the measurements in the single inter-pixel contributions, used to specify the capacitive network. The detector was simply modelled as an electrode matrix facing a metal plane, respecting the pitch, implant width and dector thickness of the different prototypes. The capacitances were obtained solving the Laplace equation with suitable boundary conditions. In fact, setting 1 V on the central pixel and grounding the neighbouring pixels and the backplane, the stored charge on each pixel numerically equals its capacitance with respect to the central pixel, having a backplane capacitance numerically equals to the stored charge on the backplane. The Laplace equation was solved in a 5×5 pixel matrix, surrounded by a guard ring, with a finite element analysis performed using the OPERA-3D package [8]. The mesh needed by the equation solver was optimised accounting for the physics aspects and the characteristics of the finite element procedure:

- because of the boundary conditions, in our model the potential should always be positive

- the charge neutrality should not be violated, i.e. the sum of the charge on all pixels and on the backplane should be zero.

- a finer mesh had to be foreseen in the regions with higher *grad* **E**.

The final optimisation was based on the minimisation of the charge neutrality violation; moreover, this was assumed as a measurement of the uncertainty on the simulation results and defines the errors in the summary table. By changing the the mesh characteristics in the high *grad* **E** region, the net effect was estimated to be at the 10% level. The results of measurements and simulation are reported in Table 4.

The consistency of the measurements is checked comparing the value obtained subtracting the measured interpixel capacitance from the measurement of $C_{ip} + C_{bp}$ (measurement I in Table 4) and the backplane capacitance from the asymptotic value in the CV curves, normalized by the number of pixels in the matrix (measurement II). The measurement cross check is satisfactory and the comparison with the calculated values is fair for all of the structures but chip 4, where difficulties both in the measurement and in the simulation were expected because of the small pitch. In particular, the maximum number of elements was preventing an optimal interpixel mesh and the extension to a larger pixel matrix, crucial for a proper interpixel capacitance evaluation of pixels with 50 μm pitch in a 350 μm thick detector. The calculated single pixel

	chip 1	chip 2	chip 3	chip 4
Implant width [μm]	100	60	50	34
Implant pitch [μm]	150	100	75	50
Readout pitch [μm]	300	200	300	200
No. of pixels in parallel	64	128	126	254
Measured C_{ip} [fF]	599±5	1038±11	958±5	2098±30
Calculated C_{ip} [fF]	630±60	880±67	690±70	980±40
Measured C_{bp} (I) [fF]	376±40	390±50	160±45	314±35
Measured C_{bp} (II) [fF]	447±5	368±5	218±5	185±5
Calculated C_{bp} [fF]	470±70	410±90	230±35	211±60

Table 4: *Interpixel (C_{ip}) and backplane (C_{bp}) capacitance values for different detector structures. The reported values refer to the specified number of pixels in parallel, corresponding to a double column of pixels, to the left and right hand side of a single bias line*

main capacitances are summarised in Table 5, together with the maximum charge loss resulting by a network analysis with a dedicated software based on the node potential method [9]. The role of the interpixel capacitance C_{ip} may be stressed referring to chip 4, where the maximum charge loss is reduced to 51% if the measured C_{ip} values are taken.

	chip 1	chip 2	chip 3	chip 4
Total C_{ip} [fF]	26.2±4.0	13.4±0.9	13.8±2.0	9.6±1.0
C_{nn} [fF]	4.4±0.7	2.0±0.1	2.1±0.3	1.5±0.2
C_{bp} [fF]	7.3±1.1	3.2±0.7	1.9±0.7	0.8±0.2
Max. charge loss	35%	32%	77%	67%

Table 5: *Single interpixel (C_{ip}), to nearest neighbour pixel (C_{nn}) and backplane (C_{bp}) capacitance values for different detector structures and estimated maximum charge loss obtained by modelling the detector as a capacitive network.*

4.3   Charge collection studies

The achievable resolution is proportional to the pixel pitch and the Noise over Signal ratio (N/S). If the implant pitch is comparable to the diffusion width, the collected charge at the output nodes will have both the contributions by the direct diffusion and the linear share by the capacitive coupling. In such a case, an improvement beyond

the binary value given by the *implant pitch*/$\sqrt{12}$ may be expected. The N/S in pixel detectors can easily exceeds 1/100, due to the small detector capacitance. Because of this, an effective signal interpolation may be expected even with $\simeq 50\%$ signal reduction.

The charge collection properties and the achievable resolution have been directly studied by shining an infrared diode spot on the backplane of a structure with 60 μm implant width, 100 μm implant pitch and 200 μm read-out pitch. At the diode wavelength of $\lambda = 880$ nm, the penetration depth in the silicon substrate corresponds to 10 μm. The IR light has been focused to a spot size of $\simeq 80$ μm and its position in the detector plane controlled by a 2-D stage allowing to scan the pixel array with micrometric accuracy. A sketch of the tested structure and the scan direction is displayed in Figure 9. A matrix of 4×7 read-out pixels has been wire-bonded to a VA-1 chip [10]. For each spot position, 1000 events have been recorded. The common mode, pedestal and noise calculation has been initialised for the first 300 events. In the subsequent events light was injected every 10 events, allowing for continuous pedestal tracking. Because of the limited data volume, no on-line suppression has been applied and the data reduction and cluster search has been performed off-line. Results have been averaged over the 70 recorded light pulses, with a peak pulse height corresponding to N/S $\simeq 1/100$ and a maximum charge loss of $\simeq 40\%$, in agreement with the network analysis. The charge sharing may be characterised by the η function, defined as $\eta = \frac{PH_i}{PH_{cluster}}$, where PH_i is the pulse height on the reference pixel i, normalised to the cluster pulse height.

The η function by construction ranges in the [0;1] interval and it has a period equals to the readout pitch. The measured pulse height and η distributions are shown in Figure 10, where the reference pixel for the first period has a centre at x $= 100$ μm. For the structure under test, the ratio between the spot size and the pitch $\simeq 0.8$ and the experimental η curve can be understood as a superposition of the effects due to the diffusion of the charge carriers created by the IR spot on the neighbouring junctions and by the capacitive charge sharing. The η parametrisation allows a coordinate reconstruction on an event by event basis and the measurement of the resolution, obtained comparing the laser spot position by the micro-metric stage to the reconstructed values. The results are shown in Figure 11.

In the interleaved pixels, where the charge sharing is most efficient, the resolution approaches $\simeq 3$ μm, irrespective of the $\simeq 40\%$ charge loss. On the other hand, when the charge sharing is minimal the resolution degrades to $\simeq 10$ μm, even with a peak pulse height. According to these results, the binary resolution defined by the *implant pitch*/$\sqrt{12}$ can be improved by about a factor 4 for a configuration where the ratio between the charge carrier cloud r.m.s. and the pixel pitch $\simeq 0.8$. A similar scaling factor can be expected for a minimum ionising particle detected by a pixel sensor with $20-25\mu m$ pitch, as long as the peak $N/S \leq 1/100$ and the charge loss is $\leq 50\%$. This would lead to an intrinsic resolution $\simeq 2\mu m$, matching well the requirements

16

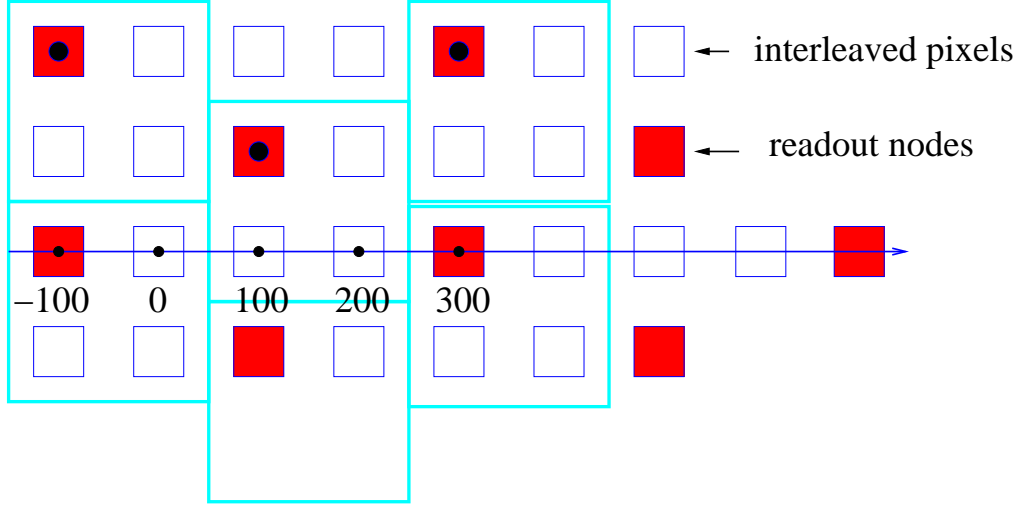Figure 9: *A sketch of the tested structure, with 100 µm implant pitch and 200 µm read-out pitch. The horizontal line identifies the scan direction and defines the coordinate system. The frames define the footprint of an hypothetical VLSI cell.*
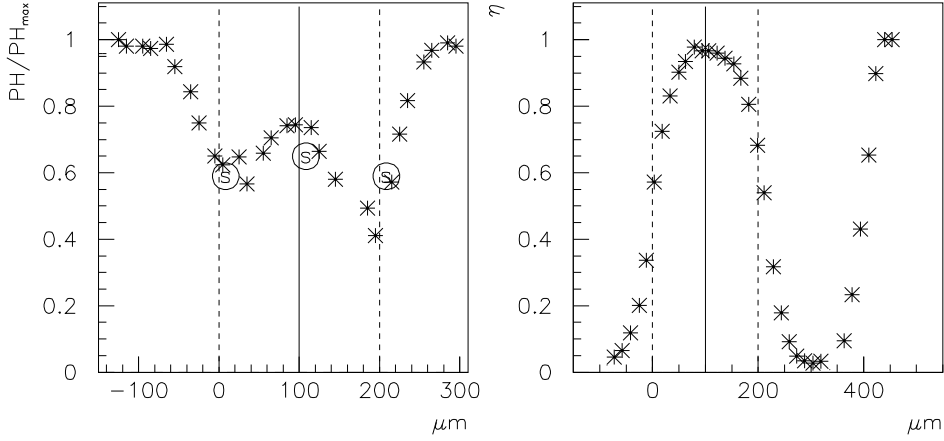

Figure 10: *The pulse height (left) and the charge sharing among neighbouring read-out pixels (right), measured by $\eta = \frac{PH_i}{PH_{tot}}$, during the detector scan. The vertical lines identify the centre of the pixels; the full line indicates the reference pixel used for the η calculation. In the left plot, the encircled "s" marks represent the predictions from the simulation.*
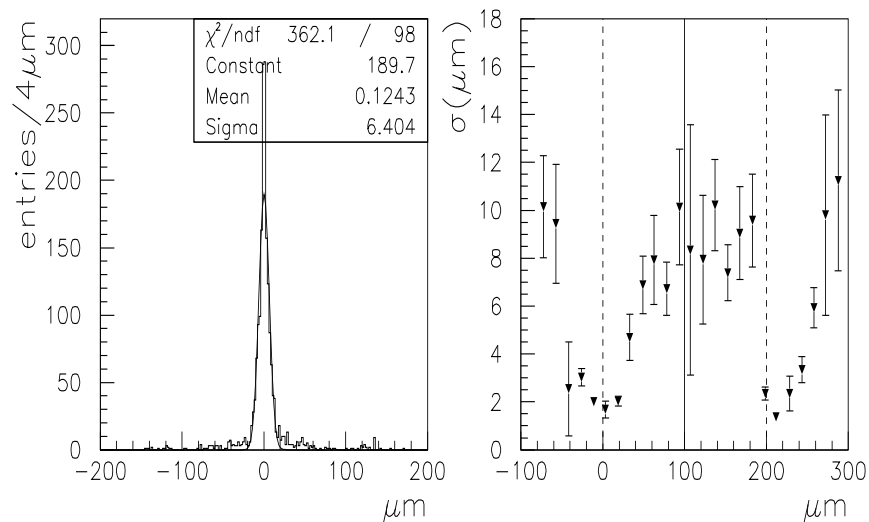
17

Figure 11: *The average resolution (left) and the achieved resolution vs. the spot position (right). The vertical lines identify the centre of the pixels; the full line indicates the reference pixel used for the η calculation*

discussed above.

5 Discussion and Conclusions

A Vertex Tracker based on a novel design of hybrid silicon pixel detectors is able to provide performances that are well adapted to the requirements of the TESLA e^+e^- collider while ensuring a significant safety margin against the influence of backgrounds. The ability to identify the individual bunch crossing of a e^+e^- event reduces the occupancy and the confusion rate from pair background and, more importantly, probability of overlap for a $\gamma\gamma \rightarrow$ hadrons event. This ensures that the identification of processes characterised by missing energy and/or heavy flavour jets at small polar angles is not confused for this underlying background [13].

The results reported in this paper conclude the feasibility study of the proposed detector concept and indicate the direction for an intense dedicated R&D programme towards a final detector design. This has to address several crucial issues:

- Sensor development. In order to achieve the desired resolution, a 25μm implant pitch detector is needed. The step from 50 to 25μm is far from being a simple scaling. In fact, because of the limited inter-pixel space, biasing by suitable polysilicon resistors is not feasible. The most promising solution is based on a

punch-through mechanism, where very small p^+ dots along the metal lines of the bias grid serve sub-matrices of four pixels. Moreover, the design has to be optimised with respect to the inter-pixel to backplane capacitance ratio, with a target charge loss below 50%. A prototype run to validate the possible solutions is planned on a short time scale; this essentially concerns small test structures, meant to be read-out with a low noise microstrip detector electronics chip;

- Electronics chip. On very general ground, each VLSI cell mating the pixel will integrate a low noise and low power charge sensitive amplifier, followed by a CR-RC shaper. Both blocks will be based on the folded cascade architecture with a PMOS transistor, chosen for its lower $1/f$ noise coefficient at its input. The analog information of the pulse height could be efficiently translated into a time-over-threshold, locally digitised on every VLSI pixel cell. Because of the low duty cycle of TESLA, a pulsed mode operation seems very well possible, thus considerably reducing the power consumption. A readout system based on a matrix sparse data scan has to be included in the design, together with time stamping of each pixel hit. The shift-register architecture proposed for the ATLAS pixel detectors could be tailored to the linear collider requirements. An end-of-column logical circuitry would deal with data packing and pipelining. The design of the chip should be optimised with the target of a cell dimension not exceeding $75 \times 75 \mu\text{m}^2$, to fully exploit the capacitive charge division mechanism. The development of a dedicated electronics chip being a considerable financial effort, this R&D phase should be considered at an advance stage of the project approval process;

- Technological development. Radiation hardening of the sensor and electronics design, back-thinning of the detector and chip, high density interconnection (flip-chip), cooling, mechanics and system integration require an experimental effort to evolve from the present conceptual design to a fully engineered study that should be planned at a later stage.

Acknowledgements

References

[1] M. Battaglia and K. Desch, to appear in the Proc. of the 5th *Int. Linear Collider Workshop*, AIP series and hep-ph/0101165.

[2] G. Borisov, private communication.

[3] T. Abe for the SLD collaboration, *Nucl. Instr. Meth.* **A447** (2000), 90.

[4] J.B.A England *et al.*, *Nucl. Instr and Meth.* **185** (1981) 43.

[5] M. Krammer and H. Pernegger, *Nucl. Instr and Meth.* **A397** (1997), 232.

[6] at the Institute of Electron Technology, Warszawa, Poland.

[7] W. Kucewicz *et al.*, *Acta Phys. Pol.* **B30** (1999) 2075.

[8] OPERA-3D, software package by Vector Fields Ltd., 24 Bankside, Kidlington, Oxon, OX5 IJE, UK.

[9] L.O. Chua and P.M. Lin, *Computed Aided Analysis of Electronic Circuits: algorithms and computational techniques*, Prentice Hall, 1975.

[10] produced by IDEAS ASA, Veritasveien 9, Box 315, N-1323 Hvik, Norway.

[11] T. Behnke *et al.*, Note LC-TOOL-2001-005.

[12] M. Elsing, Note LC-TOOL-1999-008-TESLA.

[13] M. Battaglia and D. Schulte, Note LC-PHSM-2000-052 and hep-ex/0011085.